Chemical Engineering Science 173 (2017) 253–263

Contents lists available at ScienceDirect

Chemical Engineering Science

journal homepage: www.elsevier.com/locate/ces

Highly efficient and selective absorption of H_2S in phenolic ionic liquids: A cooperative result of anionic strong basicity and cationic hydrogen-bond donation

Kuan Huang [a,b,*], Xiao-Min Zhang [c], Lin-Sen Zhou [d], Duan-Jian Tao [e,*], Jie-Ping Fan [a,b,*]

[a] Poyang Lake Key Laboratory of Environment and Resource Utilization (Nanchang University), Ministry of Education, Nanchang, Jiangxi 330031, PR China
[b] School of Resources Environmental and Chemical Engineering, Nanchang University, Nanchang, Jiangxi 330031, PR China
[c] School of Chemistry and Chemical Engineering, Nanjing University, Nanjing, Jiangsu 210093, PR China
[d] Center of Interface Dynamics for Sustainability, Institute of Materials, China Academy of Engineering Physics, Chengdu, Sichuan 610200, PR China
[e] College of Chemistry and Chemical Engineering, Jiangxi Normal University, Nanchang, Jiangxi 330022, PR China

HIGHLIGHTS

- Solubilities of H_2S and CO_2 in phenolic ionic liquids were determined.
- Phenolic ionic liquids show comparably high solubilities of H_2S.
- Solubilities of CO_2 are highly dependent on the cationic hydrogen-bond donating.
- Interactions of phenolic ionic liquids with H_2S and CO_2 were disclosed by DFT calculations.
- A strategy was proposed to design absorbents for the selective sweetening of natural gas.

ARTICLE INFO

Article history:
Received 21 April 2017
Received in revised form 6 July 2017
Accepted 31 July 2017
Available online 1 August 2017

Keywords:
Selective absorption
Hydrogen sulfide
Carbon dioxide
Phenolic ionic liquids
Hydrogen-bond donation

ABSTRACT

A series of phenolic ILs containing different cations were synthesized and investigated for the absorption of H_2S and CO_2 in this work. It is interestingly found that the solubilities of H_2S in these phenolic ILs are comparably high because of the strong interaction of basic phenolate anion with acidic H_2S, while the solubilities of CO_2 decrease significantly with the increase of cationic hydrogen-bond donation. Tetramethylguanidinium phenolate ([TMGH][PhO]), which is constructed with anion of strong basicity and cation of strong hydrogen-bond donating ability, is thus highlighted with both high solubilities of H_2S (0.56 mol/mol at 313.2 K and 0.1 bar, and 0.85 mol/mol at 313.2 K and 1 bar) and high selectivities of H_2S/CO_2 (6.2 for the ratio of H_2S solubility at 313.2 K and 0.1 bar vs. CO_2 solubility at 313.2 K and 1 bar, and 9.4 for the ratio of H_2S solubility at 313.2 K and 1 bar vs. CO_2 solubility at 313.2 K and 1 bar). Owing to the small molecular size of [TMGH][PhO], the absolute solubilities of H_2S in it (2.68 mol/kg at 313.2 K and 0.1 bar, and 4.08 mol/kg at 313.2 K and 1 bar) are particularly fascinating, and much higher than other absorbents reported in the literature. Furthermore, [TMGH][PhO] is cost-effective in comparison with other functionalized ILs specifically designed for H_2S capture, since it can be facilely synthesized from the one-step neutralization of readily available 1,1,3,3-tetramethylguanidine and phenol. The results obtained in this work indicate that [TMGH][PhO] is a promising candidate for the selective sweetening of natural gas.

1. Introduction

As the earth's reserves of coal and petroleum become more and more limited, exploring new energy resources for industrial productions and human activities is very urgent. Natural gas, whose effective component is methane (CH_4), is such an ideal candidate for its economy and cleanness (Bara, 2012). Hydrogen sulfide (H_2S) is a major contaminant in natural gas, and it is acidic, corrosive and highly toxic. Removal of H_2S is required to ensure the safety and efficiency of natural gas utilization. Absorption in aqueous organic amines is a most widely used method in the industry for natural gas sweetening (Lawson and Garst, 1976; Lee et al., 1976; Sada et al., 1976). The recycled H_2S is then catalytically

* Corresponding authors at: Poyang Lake Key Laboratory of Environment and Resource Utilization (Nanchang University), Ministry of Education, Nanchang, Jiangxi 330031, PR China.
E-mail addresses: kuan.huang@yahoo.com (K. Huang), djtao@jxnu.edu.cn (D.-J. Tao), jasperfan@163.com (J.-P. Fan).

http://dx.doi.org/10.1016/j.ces.2017.07.048
0009-2509/

converted to elemental sulfur through a well-known Claus process for easy storage and transportation (Pieplu et al., 1998). Carbon dioxide (CO_2) is normally present together with H_2S in natural gas. The absorbents for natural gas sweetening should be capable of not only selectively separating H_2S from CH_4, but also selectively separating H_2S from CO_2, in order to obtain concentrated H_2S and thereby improve the efficiency of Claus process. To this end, hindered amines (e.g., N-methyldiethanolamine and tert-butylaminoethoxyethanol) are developed for the selective sweetening of natural gas (Mandal et al., 2004; Lu et al., 2006). However, organic amines are highly volatile, corrosive and degradable, and the regeneration process is energy-intensive due to the usage of large amount of high-heat-capacity water as the diluent of absorbents. As a consequence, traditional processes for natural gas sweetening are not preferred from the viewpoint of green and sustainable chemistry.

As a class of green solvents, ionic liquids (ILs) have attracted widespread attentions over the past decades owing to their unique properties, such as distinctively ionic environment, wide liquid range, negligible volatility, high thermal stability and structural designability (Brennecke and Maginn, 2001). These features enable ILs with great potential for a variety of applications (Brennecke and Maginn, 2001), among which gas separation is particularly promising (Lei et al., 2014). The volatile loss of solvents can be significantly avoided by using ILs as the absorbents for gas separation. In addition, the energy consumption for regeneration of absorbents can be potentially reduced because of the relatively low heat capacity of ILs Fredlake et al., 2004). Therefore, the emerging of ILs offers great opportunities to address the issues associated with traditional natural gas sweetening processes employing organic amines. Within this respect, the solubilities of H_2S in various ILs constructed with a wide range of anions, including chloride ([Cl]), tetrafluoroborate ([BF_4]), hexafluorophosphate ([PF_6]), trifluoromethanesulfonate ([TfO]), bis(trifluoromethanesulfonyl)imide ([Tf_2N]), methylsulfate ([$MeSO_4$]), ethylsulfate ([$EtSO_4$]), tris(pentafluoroethyl)trifluorophosphate ([eFAP]), trifluoroacetate ([TfA]), acetate ([Ace]), lactate ([Lac]), propionate ([Pro]), glycinate ([Gly]) and alaninate ([Ala]), have been experimentally determined or theoretically simulated in previous work Jou and Mather, 2007; Pomelli et al., 2007; Jalili et al., 2009; Rahmati-Rostami et al., 2009; Jalili et al., 2010; Sakhaeinia et al., 2010a; Sakhaeinia et al., 2010b; Shiflett et al., 2010; Shiflett and Yokozeki, 2010; Shokouhi et al., 2010; Rahmati-Rostami et al., 2011; Jalili et al., 2012; Chen et al., 2013; Huang et al., 2013; Jalili et al., 2013; Mortazavi-Manesh et al., 2013; Safavi et al., 2013; Ahmadi et al., 2014; Faundez et al., 2014; Huang et al., 2014; Ji et al., 2014; Ahmadi et al., 2015; Haghtalab and Afsharpour, 2015; Haghtalab and Kheiri, 2015; Hamzehie et al., 2015; Sanchez-Badillo et al., 2015; Wang et al., 2016; Zhao et al., 2016; Afsharpour and Haghtalab, 2017; Soltani Panah, 2017; Huang et al., 2016; Huang et al., 2014). Results showed that ILs constructed with carboxylates (i.e., [Ace], [Lac] and [Pro]) or amino acid anions (i.e., [Gly] and [Ala]) exhibit much higher solubilities of H_2S than other ILs (0.35–0.70 vs. <0.05 mol/mol at 333.2 K and 1 bar) because of their chemical reactivity with H_2S (Mortazavi-Manesh et al., 2013; Wang et al., 2016; Huang et al., 2014). However, both carboxylate-based ILs and amino acid ILs also have chemical reactivity with CO_2, which results in the poor selectivities of H_2S/CO_2 in them (1.1–1.3 at 333.2 K and 1 bar) (Huang et al., 2014).

Advanced absorbents with both high solubilities of H_2S and high selectivities of H_2S/CO_2 are very fascinating for natural gas sweetening. Inspired by the chemistry of hindered amines, our group designed various ILs tethered with tertiary amine groups, specifically dual Lewis-base functionalized ILs (DLB-ILs)Huang et al., 2014 and tertiary-amine functionalized protic ILs (TA-PILs) Huang et al., 2016, for highly efficient and selective absorption of H_2S from CO_2. The principle is that there exist active protons in H_2S molecule while there do not exist active protons in CO_2 molecule, therefore, the interaction of tertiary amines with H_2S is thermodynamically and kinetically more favorable than the interaction of tertiary amines with CO_2. The solubilities of H_2S in DLB-ILs and TA-PILs at 298.2 K and 1 bar reach 0.85 and 0.55 mol/mol respectively, and the selectivities of H_2S/CO_2 in DLB-ILs and TA-PILs at 298.2 K and 1 bar reach 13.0 and 37.2 respectively. However, DLB-ILs and TA-PILs are of large molecular size, which leads to their low absolute solubilities of H_2S (in terms of mol gas/kg IL). Furthermore, the synthesis of DLB-ILs and TA-PILs are complex and involve expensive reactants, which significantly limit their large-scale productions. Another question is that besides the chemistry of hindered amines, are there any other principles that can be facilely applied to the design of functionalized ILs for natural gas sweetening?

Phenolic ILs with strong basicity were originally designed for CO_2 capture (Wang et al., 2012). By utilizing the chemical reactivity of phenolate anion ([PhO]) with CO_2, equimolar absorption of CO_2 can be achieved. It is expected that phenolic ILs are also effective for H_2S absorption because of the acidic nature of H_2S. In this work, we synthesized a series of phenolic ILs with different cations, as shown in Scheme 1. The absorption of H_2S and CO_2 in these phenolic ILs were systematically investigated. Interestingly, we found that these phenolic ILs show comparably high absorbability for H_2S, however, their absorbability for CO_2 decrease significantly with the increase of cationic hydrogen-bond donation. Thus, highly efficient and selective absorption of H_2S from CO_2 can be realized in phenolic ILs by cooperatively making use of the anionic strong basicity and cationic hydrogen-bond donation.

2. Experimental

2.1. Materials

H_2S (99.99 mol%) and CO_2 (99.99 mol%) were supplied by Nanjing Messer Gas Co. Ltd. (Nanjing, China). Tetrabutylphosphonium bromide ([P_{4444}][Br], 99 wt%) and 1-hexyl-3-methylimidazolium chloride ([hmim][Cl], 99 wt%) were purchased from Shanghai Chengjie Chemical Co. Ltd.. Diazabicyclo(5.4.0)undec-7-ene (DBU, 98 wt%), 1,1,3,3-tetramethylguanidine (TMG, 98 wt%), phenol (99 wt%) and Dowex 550 A hydroxide form anion exchange resin were purchased from Sigma Aldrich Co. Ltd.. All the chemicals were used directly without further purification.

2.2. Synthesis

[P_{4444}][PhO] and [hmim][PhO] were prepared by a two-step route: the ethanolic solutions of halide precursors were passed through a column filled with Dowex 550 A hydroxide form anion exchange resin to produce corresponding hydroxides, and then the hydroxides were neutralized by stoichiometric phenol to produce corresponding ILs. [DBUH][PhO] and [TMGH][PhO] were prepared by a one-step route: the ethanolic solutions of cationic sources were directly neutralized by stoichiometric phenol to produce corresponding ILs. Most of the solvents were removed by rotary evaporation, and the crude ILs were dried under vacuum at 353.2 K for 48 h to offer final products.

The water contents in phenolic ILs were examined to be less than 0.1 wt% by a 787KF Titrino instrument. The halide residues in phenolic ILs were determined to be less than 0.1 wt% through Mohr titration.

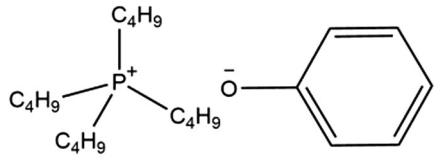

tetrabutylphosphonium phenolate ([P_{4444}][PhO])

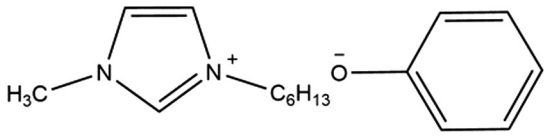

1-hexyl-3-methylimidazolium phenolate ([hmim][PhO])

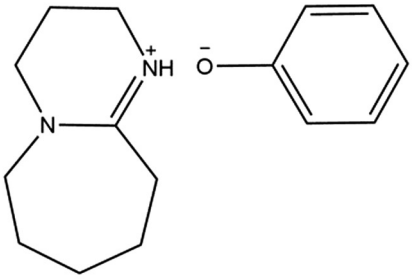

1,8-diazabicyclo[5.4.0]undec-7-ene-1-ium phenolate ([DBUH][PhO])

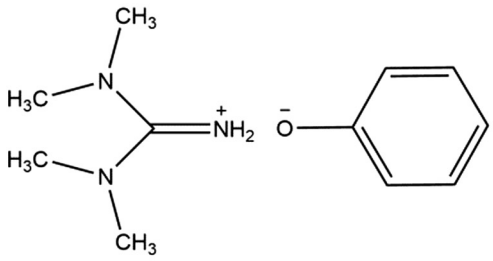

tetramethylguanidinium phenolate ([TMGH][PhO])

Scheme 1. Chemical structures of phenolic ILs synthesized in this work.

2.3. Characterizations

The synthesized phenolic ILs were characterized by ^{1}H NMR spectra, ^{13}C NMR spectra, FTIR spectra, ESI-MS, elemental analysis and TG-DSC. ^{1}H NMR and ^{13}C NMR spectra were collected on a Bruker DPX 300 MHz spectrometer using CD_3Cl as the solvent and TMS as the internal standard. FTIR spectra were collected on a Nicolet NEXUS870 spectrometer. ESI-MS were collected on a Shimadazu LCMS 2020 instrument. Elemental analysis were performed on a Heraeus CHN-O-Rapid instrument. TG-DSC traces were collected on a Netzsch STA 449 C instrument from room temperature to 873.2 K at a heating rate of 10 K/min under N_2 to determine the decomposition temperatures of phenolic ILs; DSC traces were further collected on the same instrument from 223.2 to 323.2 K at a heating rate of 10 K/min under N_2 to determine the melting temperatures and glass transition temperatures of phenolic ILs. Characterization results are presented in the Supplementary Materials (see Figs. S1–S21), and summarized as below:

[P_{4444}][PhO] ^{1}H NMR (300 MHz, CD_3Cl, 298.2 K, TMS), δ (ppm): 0.91 (3H, t), 1.41 (16H, m), 2.19 (8H, t), 6.59 (2H, m), 6.87 (2H, d), 7.05 (1H, m); ^{13} C NMR (300 MHz, CD_3Cl, 298.2 K, TMS), δ (ppm): 13.4, 18.9, 27.1, 28.0, 116.6, 116.8, 129.1, 160.5; FTIR, $\bar{\upsilon}$ (cm^{-1}): 516, 550, 617, 692, 760, 823, 907, 987, 1096, 1159, 1243, 1314, 1381, 1407, 1469, 1587, 2871, 2935, 2957, 3053, 3414; ESI-MS, calculated for $C_{16}H_{36}P^+$: 259.25, found: 259.33, calculated for $C_6H_5O^-$: 93.03, found: 93.00; elemental analysis, calculated for $C_{22}H_{41}OP$: C 74.95%, H 11.72%, found: C 74.81%, H 11.66%; TG-DSC, decomposition temperature: 488 K; DSC, melting temperature and glass transition temperature: not found at 223.2–323.3 K.

[hmim][PhO] ^{1}H NMR (300 MHz, CD_3Cl, 298.2 K, TMS), δ (ppm): 0.83 (3H, t), 1.17–1.25 (6H, m), 1.67 (2H, m), 3.76 (3H, s), 3.96 (2H, t), 6.58 (2H, m), 6.79 (2H, d), 7.03 (1H, m), 7.11 (2H, d), 8.85 (1H, s); ^{13} C NMR (300 MHz, CD_3Cl, 298.2 K, TMS), δ (ppm): 13.9, 22.4, 25.8, 30.1, 31.0, 49.9, 116.4, 116.9, 121.5, 123.2, 129.3, 161.5; FTIR, $\bar{\upsilon}$ (cm^{-1}): 522, 620, 655, 695, 764, 822, 874, 989, 1024, 1070, 1167, 1294, 1398, 1484, 1583, 1663, 1859, 2933, 2958, 3152, 3403; ESI-MS, calculated for $C_{10}H_{19}N_2^+$: 167.28, found: 167.17, calculated for $C_6H_5O^-$: 93.03, found: 93.00; elemental analysis, calculated for $C_{16}H_{24}N_2O$: C 73.81%, H 9.29%, N 10.76, found: C 73.78%, H 9.50%, N 10.18%; TG-DSC, decomposition temperature: 519 K; DSC, melting temperature and glass transition temperature: not found at 223.2–323.3 K.

[DBUH][PhO] ^{1}H NMR (300 MHz, CD_3Cl, 298.2 K, TMS), δ (ppm): 1.56–1.64 (6H, m), 1.82 (2H, m), 2.49 (2H, m), 3.23–3.30 (6H, m), 6.68 (2H, m), 6.82 (2H, d), 7.12 (1H, m); ^{13}C NMR (300 MHz, CD_3Cl, 298.2 K, TMS), δ (ppm): 21.4, 25.2, 27.9, 30.0, 34.6, 41.3, 48.3, 53.2, 116.7, 116.8, 129.2, 161.1, 163.4; FTIR, $\bar{\upsilon}$ (cm^{-1}): 516, 550, 619, 696, 764, 820, 880, 987, 1069, 1112, 1163, 1206, 1275, 1326, 1365, 1476, 1584, 1609, 1644, 2858, 2932, 3053, 3254, 3394; ESI-MS, calculated for $C_9H_{17}N_2^+$: 153.14, found: 153.08, calculated for $C_6H_5O^-$: 93.03, found: 93.00; elemental analysis, calculated for $C_{15}H_{22}N_2O$: C 73.13%, H 9.00%, N 11.37, found: C 73.73%, H 9.16%, N 10.82%; TG-DSC, decomposition temperature: 538 K; DSC, melting temperature and glass transition temperature: not found at 223.2–323.3 K.

[TMGH][PhO] ^{1}H NMR (300 MHz, CD_3Cl, 298.2 K, TMS), δ (ppm): 2.75 (12H, s), 6.73 (2H, m), 6.88 (2H, d), 7.15 (1H, m), 8.95 (2H, s); ^{13} C NMR (300 MHz, CD_3Cl, 298.2 K, TMS), δ (ppm): 39.3, 116.6, 117.6, 129.4, 159.9, 166.1; FTIR, $\bar{\upsilon}$ (cm^{-1}): 515, 554, 616, 695, 760, 822, 883, 989, 1037, 1063, 1103, 1164, 1248, 1274, 1410, 1476, 1590, 1661, 2601, 2941, 3013, 3054, 3158, 3334; ESI-MS, calculated for $C_5H_{14}N_3^+$: 116.12, found: 116.08, calculated for $C_6H_5O^-$: 93.03, found: 93.00; elemental analysis, calculated for $C_{11}H_{19}N_3O$: C 63.13%, H 9.15%, N 20.08, found: C 63.37%, H 9.01%, N 20.94%; TG-DSC, decomposition temperature: 481 K; DSC, melting temperature and glass transition temperature: not found at 223.2–323.3 K.

The densities of phenolic ILs were measured on an Anton Paar DMA 5000 densiometer with a precision of 0.00001 g/cm^3. The viscosities of phenolic ILs were measured on a Brookfield LVDV-II + Pro viscometer with an uncertainty of ±1% in relation to the full scale.

2.4. Measurement of gas solubility

The apparatus for measuring gas solubilities in phenolic ILs is the same as that reported in our previous work (Huang et al., 2013; Huang et al., 2014; Huang et al., 2016). The whole device consists of two 316 L stainless steel chambers whose volumes are 120.802 cm^3 (V_1) and 47.368 cm^3 (V_2), respectively. The bigger chamber, used as gas reservior, isolates the gas before it contacts with the IL in the smaller chamber. The smaller chamber, named as equilibrium cell, is equipped with a magnetic stirrer. The temperatures (T) of both chambers are controlled using a water bath

with an uncertainty of ±0.1 K. The pressures in two chambers are monitored using two pressure transducers with an uncertainty of ±0.2% (in relation to the full scale). The pressure transducers are connected to a numeric instrument to record the pressure changes online. In a typical run, a known mass (w) of IL was placed into the equilibrium cell, and the air in two chambers was evacuated. The remaining pressure in equilibrium cell was recorded to be P_0 (<0.001 bar). The gas from cylinder was then fed into the gas reservior to a pressure of P_1. The needle valve between the two chambers was turned on to let the gas be introduced to the equilibrium cell. Absorption equilibrium was thought to be reached when the pressures of two chambers remained constant for at least 2 h. The equilibrium pressures were denoted as P_2 for the equilibrium cell and P'_1 for the gas reservior. The gas partial pressure in the equilibrium cell was $P_g = P_2 - P_0$. The gas uptake, $n(P_g)$, can thus be calculated using equation (1):

$$n(P_g) = \rho_g(P_1, T)V_1 - \rho_g(P'_1, T)V_1 - \rho_g(P_g, T)(V_2 - w/\rho_{IL}) \quad (1)$$

where ρ_g (P_i,T) represents the density of gas in mol/cm^3 at P_i (i = 1, g) and T. ρ_{IL} is the density of IL in g/cm^3 at T. V_1 and V_2 represent the volumes in cm^3 of two chambers, respectively. Continual measurements of solubility data at elevated pressures were performed by introducing more gas into the equilibrium cell to reach new equilibrium. The solubility of gas was defined in terms of mol gas/mol IL or mol gas/kg IL in this work. After measurements, the gas remaining in chambers were swept to an off-gas absorber containing aqueous solution of NaOH to prevent the gas from leaking into the atmosphere. Duplicate experiments were run for each IL to obtain averaged values of gas solubility. The reproducibility of solubility data in this work was well within ±1%.

2.5. Theoretical calculations

Density function theory (DFT) calculations were performed with a Gaussian 09 program (Frisch et al. 2009). All the geometries were fully optimized at the B3LYP/6-31G++(d,p) level of theory. To incorporate a polar environment for ILs and IL-gas complexes, a polarizable continuum model (PCM) with water as the solvent was used, since ILs have been previously determined to have comparable polarity as water (Greaves and Drummond, 2008). Frequency calculations were performed to confirm the true minima. For each IL and IL-gas complex, structures with different binding modes were screened to locate the most stable structure.

3. Results and discussion

3.1. Physical properties of different phenolic ILs

Densities and viscosities are fundamental data of absorbents and very important for the process design of natural gas sweetening. Fig. 1 shows the densities and viscosities of different phenolic ILs at the temperatures of 303.2–353.2 K. The densities of the four phenolic ILs synthesized in this work are 0.95394–1.110520 cm^3/g at 303.2 K, with the lowest for [P_{4444}][PhO] and the highest for [DBUH][PhO]. The viscosities are 125.7–435.1 cp at 303.2 K, with the lowest for [TMGH][PhO] and the highest for [hmim][PhO]. The densities of phenolic ILs decrease almost linearly, while the viscosities of phenolic ILs decrease non-linearly, with the increase of temperature. The density and viscosity data can be fitted by linear Eq. (2) and VFT Eq. (3) respectively:

$$\rho = a + bT \quad (2)$$

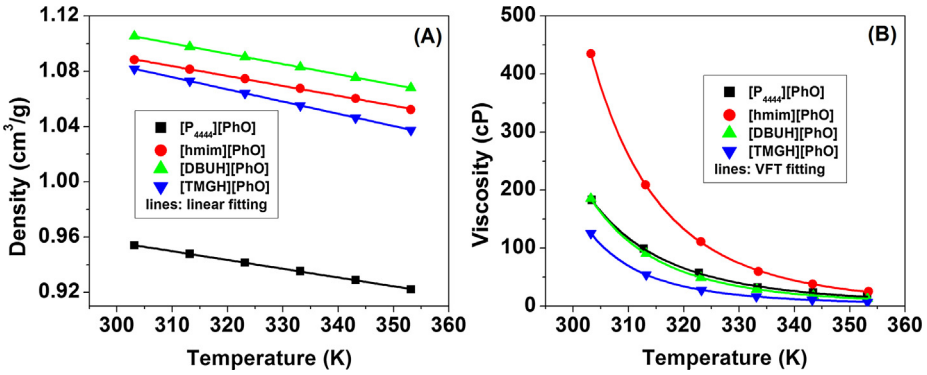

Fig. 1. Densities (A) and viscosities (B) of different phenolic ILs.

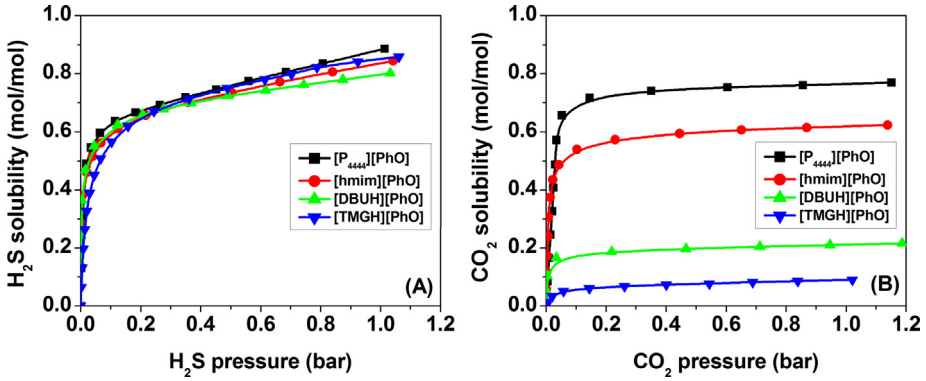

Fig. 2. Absorption isotherms of H_2S (A) and CO_2 (B) in different phenolic ILs at 313.2 K.

$$\eta = \eta_0 \exp\left(\frac{D}{T - T_0}\right) \quad (3)$$

In Eqs. (2) and (3), ρ is the density in cm^3/g, η is the viscosity in cP, T is the temperature in K, a, b, η_0, D and T_0 are empirical parameters. Fitting results are summarized in Table S1 in the Supplementary Materials.

3.2. Solubilities of H_2S and CO_2 in different phenolic ILs

Fig. 2 shows the absorption isotherms of H_2S and CO_2 in different phenolic ILs at 313.2 K, and Table 1 summarizes the solubilities of H_2S at 0.1 and 1 bar and the solubilities of CO_2 at 1 bar. Herein, the gas solubility data are expressed in terms of mol gas/mol IL to reasonably compare the interaction of different phenolic ILs with H_2S and CO_2. Obviously, the four phenolic ILs show comparably high absorbability for H_2S, with the solubilities of H_2S approaching ~0.60 mol/mol at 0.1 bar and ~0.85 mol/mol 1 bar. The isothermal profiles of H_2S absorption in phenolic ILs are non-ideally chemical types, implying the strong interaction of phenolic ILs with H_2S. This is within expectation since [PhO] is with strong basicity while H_2S is with weak acidity. However, it is surprisingly found that the four phenolic ILs show varied absorbability for CO_2, with the sequence of $[P_{4444}][PhO] > [hmim][PhO] > [DBUH][PhO] > [TMGH][PhO]$. For example, $[P_{4444}][PhO]$ can absorb as high as 0.77 mol/mol of CO_2 at 1 bar, while [hmim][PhO], [DBUH][PhO] and [TMGH][PhO] can absorb only 0.62, 0.21 and 0.090 mol/mol of CO_2 at the same pressure. It is necessary to figure out what factor determines the varied solubility of CO_2 in the four phenolic ILs.

The high solubilities of CO_2 in $[P_{4444}][PhO]$ have been previously validated as a result of the strong chemical reactivity of [PhO] with

Table 1
p*K*a of cations, solubilities of H_2S and CO_2 and selectivities of H_2S/CO_2 in phenolic ILs[a].

Phenolic ILs	p*K*a of cations[b]	$R_{H2S,0.1}$[c] (mol/mol)	$R_{H2S,1}$[d] (mol/mol)	$R_{CO2,1}$[e] (mol/mol)	$S_{0.1/1}$[f]	$S_{1/1}$[g]
$[P_{4444}][PhO]$	42.0[h] (Zhang et al., 1993)	0.62	0.88	0.77	0.81	1.1
[hmim][PhO]	21.1 (32.4)[i] (Magill et al., 2004)	0.59	0.84	0.62	1.0	1.4
[DBUH][PhO]	(24.3) (Kaljurand et al., 2000)	0.60	0.80	0.21	2.9	3.8
[TMGH][PhO]	(23.4) (Lide, 2003)	0.56	0.85	0.090	6.2	9.4

[a] p*K*a were reported at 298.2 K; solubility data were determined at 313.2 K.
[b] p*K*a outside parentheses were reported in DMSO; p*K*a inside parentheses were reported in MeCN.
[c] Solubility of H_2S at 0.1 bar.
[d] Solubility of H_2S at 1 bar.
[e] Solubility of CO_2 at 1 bar.
[f] Selectivity of H_2S/CO_2 defined as $R_{H2S,0.1}/R_{CO2,1}$.
[g] Selectivity of H_2S/CO_2 defined as $R_{H2S,1}/R_{CO2,1}$.
[h] p*K*a of $[N_{1111}]$.
[i] p*K*a of [mmim].

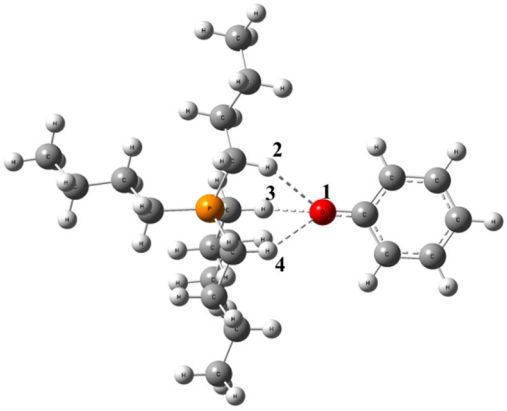

$[P_{4444}][PhO]$ (bond length in Å : O_1---H_2, 2.415; O_1---H_3, 2.320; O_1---H_4, 2.304)

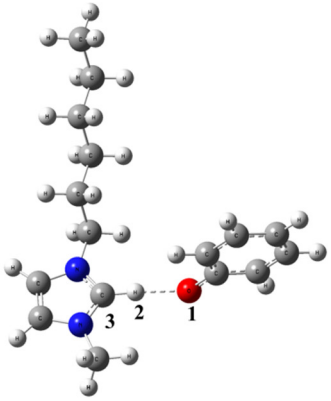

[hmim][PhO] (bond length in Å : O_1---H_2, 1.797; C_3---H_2, 1.108)

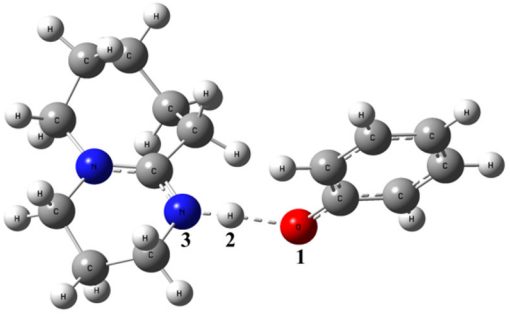

[DBUH][PhO] (bond length in Å : O_1---H_2, 1.552; N_3---H_2, 1.077)

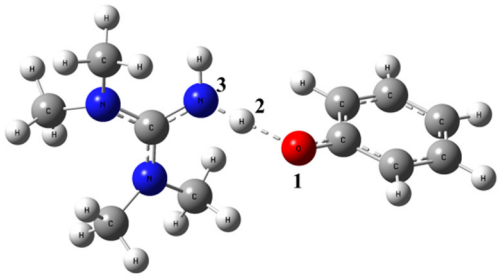

[TMGH][PhO] (bond length in Å : O_1---H_2, 1.515; N_3---H_2, 1.090)

Fig. 3. Optimized structures of phenolic ILs.

CO_2 (Zhang et al., 2015). The transition state for the reaction of [PhO] with CO_2 was also identified by DFT calculations in this work. As shown in Fig. S22, very low activation energy (1.9 kJ/mol) and exothermic interaction energy (−40.3 kJ/mol) were demonstrated, further verifying the strong chemical reactivity of [PhO] with CO_2. Accordingly, the significantly reduced solubilities of CO_2 in other three phenolic ILs must be related to weakened interaction of [PhO] with CO_2 as phenolic oxygen is the only active site for trapping CO_2. Since [PhO] is with strong basicity, it tends to attract active protons. Therefore, [PhO] would interact with cations containing active protons strongly by forming O---H hydrogen bonds. The donation of hydrogen bonds from cations to [PhO] should decrease its ability to trap CO_2, thus causing the sacrifice of CO_2 solubility. By carefully analyzing the structures of the four phenolic ILs, it is found that their cations have different hydrogen-bond donating ability. The thermodynamic dissociation constants (pK_a) are indicators of the strength of acidity, and thereby can be used to reflect the relative hydrogen-bond donating ability (Shang et al., 2017). Lower is the pK_a, stronger the hydrogen-bond donating ability is. The pK_a of [P_{4444}] (αC—H bond), [hmim] (C2—H bond), [DBUH] (N—H bond) Kaljurand et al., 2000 and [TMGH] (N—H bond) Lide, 2003 in dimethylsulfoxide (DMSO) or acetonitrile (MeCN) are presented in Table 1. It should be noted that the pK_a of [P_{4444}] and [hmim] are not available in the literature. Herein, the pK_a of tetramethylammonium ([N_{1111}]) Zhang et al., 1993 and 1-methyl-3-methylimidazolium ([mmim]) Magill et al., 2004 are taken for approximate comparison. This approximation is reasonable since the electronic environments of αC—H bond in [N_{1111}] and C2—H bond in [mmim] are similar to those in [P_{4444}] and [hmim], respectively. From the pK_a of different cations, it can be seen that the sequence of hydrogen-bond donating ability is [P_{4444}] < [hmim] < [DBUH] < [TMGH]. It is clearly shown in Table 1 that the solubilities of CO_2 in phenolic ILs decrease significantly with the increase of cationic hydrogen-bond donating ability.

Based on the experimental observation and qualitatively analysis, it is deduced that the strong interaction of phenolic ILs with H_2S is independent on the hydrogen-bond donating ability of cations, while the interaction of phenolic ILs with CO_2 is highly dependent on the hydrogen-bond donating ability of cations.

3.3. Interaction of different phenolic ILs with H_2S and CO_2

To understand why the dependence of H_2S solubilities and CO_2 solubilities in phenolic ILs on the cationic hydrogen-bond donation show different trends at the molecular level, DFT calculations were performed to optimize the structures of phenolic ILs and phenolic IL-gas complexes. Fig. 3 shows the most stable structures of different phenolic ILs. It can be clearly seen that hydrogen bonds are formed between the active protons of cations and phenolic oxygen. The attraction of active protons by [PhO] even causes the partial dissociation of [DBUH] and [TMGH]. The lengths of hydrogen bonds are 2.304–2.415 Å in [P_{4444}][PhO], 1.797 Å in [hmim][PhO], 1.552 Å in [DBUH][PhO] and 1.515 Å in [TMGH][PhO] respectively, indicating that the strength of hydrogen bonds follow the sequence of [P_{4444}][PhO] < [hmim][PhO] < [DBUH][PhO] < [TMGH][PhO]. This is in consistence with the sequence of cationic hydrogen-bond donating ability concluded from the comparison of cationic pK_a values.

Fig. 4 shows the most stable structures of phenolic IL-H_2S complexes. H_2S is also a hydrogen-bond donor. The donation of

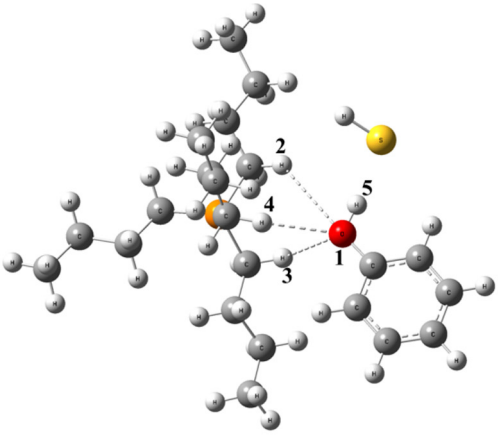

[P_{4444}][PhO]-H_2S (bond length in Å : O_1---H_2, 3.431; O_1---H_3, 3.120; O_1---H_4, 2.434; O_1—H_5, 1.003), Δ*H*=-53.1 kJ/mol

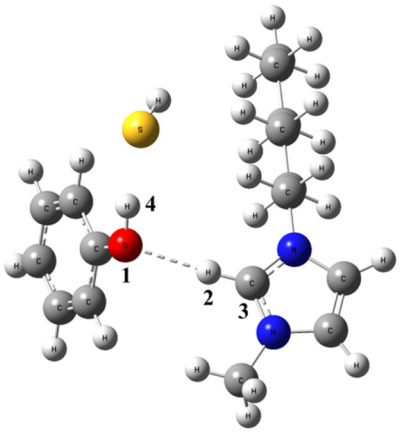

[hmim][PhO]-H_2S (bond length in Å : O_1---H_2, 2.105; C_3—H_2, 1.086; O_1—H_4, 1.007), Δ*H*=-47.6 kJ/mol

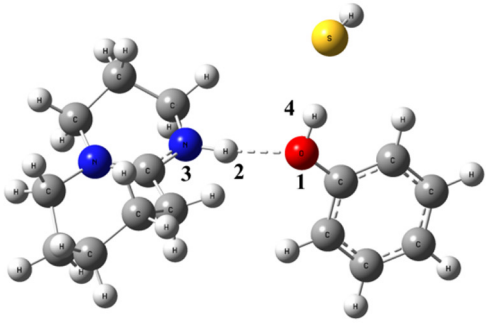

[DBUH][PhO]-H_2S (bond length in Å : O_1---H_2, 1.892; N_3—H_2, 1.023; O_1—H_4, 1.011), Δ*H*=-31.7 kJ/mol

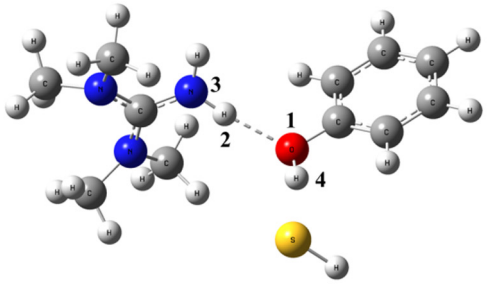

[TMGH][PhO]-H_2S (bond length in Å : O_1---H_2, 1.903; N_3—H_2, 1.023; O_1—H_4, 1.010), Δ*H*=-31.9 kJ/mol

Fig. 4. Optimized structures of phenolic IL + H_2S complexes.

hydrogen bonds from H_2S to [PhO] and from cations to [PhO] are two competing processes. The hydrogen-bond donating ability of H_2S is much stronger than the four cations of phenolic ILs since its pK_{a1} is 6.89 (298.2 K, in water). Therefore, [PhO] prefers to attract the active protons of H_2S. On the other hand, the active protons of H_2S are ionizable in the presence of [PhO], which is with strong basicity. As a result, the active protons of H_2S attach to the phenolic oxygen to form solid O—H bonds, the lengths of which are 1.003–1.011 Å. Table S2 summarizes the Mulliken charge numbers of S in H_2S and phenolic oxygen in phenolic ILs before and after phenolic ILs interact with H_2S. As can be seen, the charge numbers are −0.920 to −0.860 on S and −0.480 to −0.379 on phenolic oxygen in phenolic IL-H_2S complexes, while the charge numbers are -0.254 on S in H_2S and −0.756 to −0.710 on phenolic oxygen in phenolic ILs. The change in charge distributions is in consistence with the breakage of H—S bonds in H_2S and formation of O—H bonds in phenolic ILs. Correspondingly, the active protons of cations are excluded back to the cations. The hydrogen bonds between the active protons of cations and phenolic oxygen are thus extended to 2.434–3.431 Å in [P_{4444}][PhO]-H_2S, 2.105 Å in [hmim][PhO]-H_2S, 1.892 Å in [DBUH][PhO]-H_2S and 1.903 Å in [TMGH][PhO]-H_2S respectively, being longer than those in pristine phenolic ILs. Furthermore, the active protons of H_2S and [PhO] form coplanar structures, making the phenolic IL-H_2S complexes thermodynamically stable. The enthalpy change for the interaction of phenolic ILs with H_2S, which were obtained by substracting the enthalpies of IL and gas from the enthalpy of IL-gas complex, are −53.1 kJ/mol for [P_{4444}][PhO]-H_2S, −47.6 kJ/mol for [hmim][PhO]-H_2S, −31.7 kJ/mol for [DBUH][PhO]-H_2S and −31.9 kJ/mol for [TMGH][PhO]-H_2S, respectively. The highly exothermic enthalpy change validate the strong interaction of phenolic ILs with H_2S, which has been disclosed by the non-ideal profiles of H_2S absorption isotherms shown in Fig. 2A. It should be noted that it is difficult to verify the mechanism of H_2S absorption in phenolic ILs by experiments, as only proton transfer takes place in this system. Furthermore, H_2S is highly toxic; as a result, it is not safe to perform other advanced characterizations. Anyway, the DFT calculation results are generally in consistence with the acid-base theory.

Fig. 5 shows the most stable structures of phenolic IL-CO_2 complexes. As a Lewis acid, CO_2 is also attractive to [PhO]. However, CO_2 is non-ionizable because of the absence of active protons. Therefore, the CO_2 molecule attaches to the phenolic oxygen as an entirety. The transfer of electrons from electron-rich phenolic oxygen to election-deficient carbon of CO_2 results in the formation of solid O—C bonds, the lengths of which are 1.443–1.465 Å. Simultaneously, the CO_2 molecule transforms from linear structure to angular structure. Unlike the coplanar structures of active protons of H_2S and [PhO], the angular CO_2 and [PhO] form non-coplanar structures, making the phenolic IL-CO_2 complexes less thermodynamically stable than phenolic IL-H_2S complexes. The mechanism of CO_2 absorption in phenolic ILs, in which the interaction of phenolic oxygen with CO_2 plays an important role and carbonate is formed, has been well established both experimentally and theoretically in the literature (Wang et al., 2012). The DFT calculation results obtained in this work also demonstrate the strong interaction of phenolic oxygen with CO_2.

It can be further observed from Fig. 5 that the hydrogen bonds O_1---H_3 and O_1---H_4 in [P_{4444}][PhO] and O_1---H_2 in [hmim][PhO] are broken after the introduction of CO_2 due to the weak hydrogen-bond donating ability of [P_{4444}] and [hmim]. In contrast,

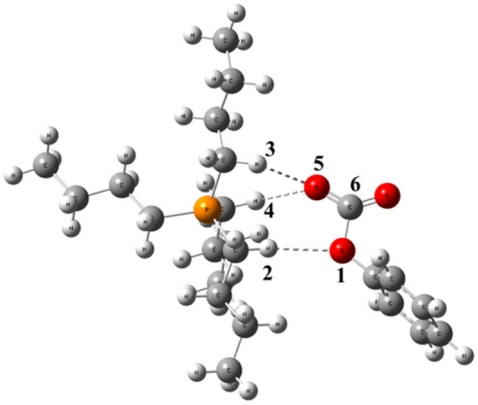

[P_{4444}][PhO]-CO_2 (bond length in Å : O_1---H_2, 2.449; O_5---H_3, 2.484; O_5---H_4, 2.381; O_1—C_6, 1.447), ΔH=-35.3 kJ/mol

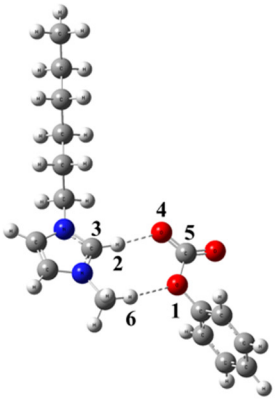

[hmim][PhO]-CO_2 (bond length in Å : O_1---H_6, 2.402; C_3—H_2, 1.094; O_4---H_2, 1.942; O_1—C_5, 1.443), ΔH=-33.5 kJ/mol

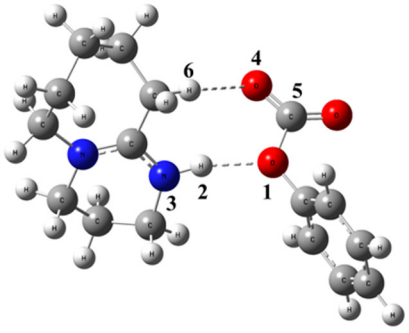

[DBUH][PhO]-CO_2 (bond length in Å : O_1---H_2, 1.913; N_3—H_2, 1.023; O_1—C_5, 1.463, O_4---H_6, 2.323), ΔH=-12.0 kJ/mol

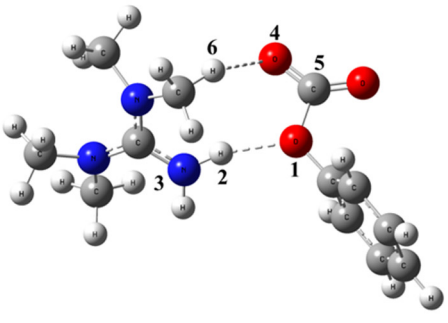

[TMGH][PhO]-CO_2 (bond length in Å : O_1---H_2, 1.906; N_3—H_2, 1.023; O_1—C_5, 1.465, O_4---H_6, 2.527), ΔH=-11.4 kJ/mol

Fig. 5. Optimized structures of phenolic IL + CO_2 complexes.

the hydrogen bonds O_1---H_2 in [DBUH][PhO] and O_1---H_2 in [TMGH][PhO] are not broken after the introduction of CO_2 due to the strong hydrogen-bond donating ability of [DBUH] and [TMGH]. The breaking of hydrogen bonds between the active protons of cations and phenolic oxygen has two favorable effects on the interaction of phenolic ILs with CO_2. First, the phenolic oxygen with strong basicity is released to complex with CO_2 efficiently. As a consequence, the O—C bonds between the phenolic oxygen and carbon of angular CO_2 in [P_{4444}][PhO]-CO_2 and [hmim][PhO]-CO_2 are shorter than those in [DBUH][PhO]-CO_2 and [TMGH][PhO]-CO_2 (1.447–1.443 *vs.* 1.463–1.465 Å). Second, the reconfiguration of active protons of cations results in the formation of new and strong hydrogen bonds between the oxygen of angular CO_2 and active protons of cations, i.e., O_5---H_3 and O_5---H_4 in [P_{4444}][PhO]-CO_2 and O_4---H_2 in [hmim][PhO]-CO_2, the lengths of which are 2.484, 2.381 and 1.942 Å respectively. As a consequence, the non-coplanar structures of angular CO_2 and [PhO] are stabilized and the energy of [P_{4444}][PhO]-CO_2 and [hmim][PhO]-CO_2 are reduced. However, the oxygen of angular CO_2 can only form very week hydrogen bonds with the adjacent protons of cations, i.e., O_4---H_6 in [DBUH][PhO]-CO_2 and O_4---H_6 in [TMGH][PhO]-CO_2, the lengths of which are 2.323 and 2.527 Å respectively. As a result, the enthalpy change for the interaction of [P_{4444}][PhO] and [hmim][PhO] with CO_2 are still highly exothermic with the values calculated to be −35.3 and −33.5 kJ/mol respectively, while the enthalpy change for the interaction of [DBUH][PhO] and [TMGH][PhO] with CO_2 are only slightly exothermic with the values calculated to be −12.0 and −11.4 kJ/mol respectively.

Based on the DFT calculation results, it is concluded that the hydrogen-bond donation of cations plays the key role in differentiating the interaction of phenolic ILs with H_2S and CO_2. Since H_2S is ionizable and the active protons of H_2S can form relatively stable coplanar structures with [PhO], the hydrogen-bond donating ability of cations has negligible effect on the strong interaction of phenolic ILs with H_2S. However, CO_2 is non-ionizable and the angular CO_2 forms relatively unstable non-coplanar structures with [PhO], making the interaction of phenolic ILs with CO_2 rather sensitive to the hydrogen-bond donating ability of cations. For phenolic ILs with weakly cationic hydrogen-bond donation, they can still interact with CO_2 strongly by restructuring of hydrogen-bond networks. Nonetheless, for phenolic ILs with strongly cationic hydrogen-bond donation, they can only interact with CO_2 very weakly since the hydrogen-bond networks can hardly be restructuring.

3.4. Selectivities of H_2S/CO_2 in different phenolic ILs

The selectivities of H_2S/CO_2 in different phenolic ILs are then calculated and summarized in Table 1. Considering that the content of H_2S varies significantly in different natural gas sources, two kinds of ideal selectivity were defined in this work:

$$S_{0.1/1} = R_{H2S,0.1}/R_{CO2,1} \quad (4)$$

$$S_{1/1} = R_{H2S,1}/R_{CO2,1} \quad (5)$$

$S_{0.1/1}$ is used for evaluating the ability of phenolic ILs to selectively absorb low-content H_2S from CO_2, and $S_{1/1}$ is used for evaluating the ability of phenolic ILs to selectively absorb high-content H_2S from CO_2. Owing to the different trends for the dependence of H_2S solubilities and CO_2 solubilities in phenolic ILs on the cationic hydrogen-bond donation, phenolic ILs with weakly cationic hydrogen-bond donation display poor selectivities of H_2S/CO_2 while phenolic ILs with strongly cationic hydrogen-bond donation display high selectivities of H_2S/CO_2. For example, the values of $S_{0.1/1}$ and $S_{1/1}$ in [P_{4444}][PhO] are 0.81 and 1.1 respectively, while those in [TMGH][PhO] reach 6.2 and 9.4 respectively. Therefore, [TMGH][PhO] can be potentially used for the selective absorption of H_2S from CO_2, while the other three phenolic ILs cannot.

3.5. Comparison of phenolic ILs with other absorbents

To thoroughly compare the potential of different absorbents for the selective sweetening of natural gas, the solubilities of H_2S and selectivities of H_2S/CO_2 in other absorbents reported in the literature including carboxylate-based ILs (e.g., [emim][Ac]) Huang et al., 2013; Shiflett and Yokozeki, 2009, amino acid ILs (e.g., [N_{2224}][Gly]) (Huang et al., 2014), DLB-ILs (e.g., [N_{2224}][IMA] and [N_{2224}][NIA]) (Huang et al., 2014), TA-PILs (e.g., [BDMAEE][Tf_2 N] and [TMHDA][Tf_2 N]) (Huang et al., 2016), protic ILs (e.g., [DMEAH][Ac] and [DMEAH][For]) (Huang et al., 2014), normal ILs (e.g., [emim][Tf_2 N]) Sakhaeinia et al., 2010a; Hong et al., 2007 and industrially used MDEA (Koech et al., 2011; Jou et al., 1982) are summarized in Table 2. From the comparison, it can be clearly seen that the solubilities of H_2S in [TMGH][PhO] (0.56 mol/mol at 0.1 bar and 0.85 mol/mol at 1 bar) are higher than those in other absorbents reported in the literacture (0.006–0.59 mol/mol at 0.1 bar and 0.060–0.85 mol/mol at 1 bar). The selectivities of H_2S/CO_2 in [TMGH][PhO] (6.2 for $S_{0.1/1}$ and 9.4 for $S_{1/1}$) are satisfactorily

Table 2
Solubilities of H_2S and CO_2 and selectivities of H_2S/CO_2 in absorbents reported in the literature.[a]

Absorbents	$R_{H2S,0.1}$[b] (mol/mol)	$R_{H2S,1}$[c] (mol/mol)	$R_{CO2,1}$[d] (mol/mol)	$S_{0.1/1}$[e]	$S_{1/1}$[f]
[emim][Ac][g] (Huang et al., 2013; Shiflett and Yokozeki, 2009)	0.20	0.41	0.30	0.67	1.4
[N_{2224}][Gly][h] (Huang et al., 2014)	0.59	0.66	0.59	1.0	1.1
[N_{2224}][IMA] (Huang et al., 2014)	0.16	0.51	0.031	5.2	16.5
[N_{2224}][NIA] Huang et al., 2014	0.12	0.56	0.031	3.9	18.1
[BDMAEE][Tf_2N] (Huang et al., 2016)	0.11	0.44	0.013	8.5	33.8
[TMHDA][Tf_2N] Huang et al., 2016	0.24	0.67	0.023	10.4	29.1
[DMEAH][Ac] (Huang et al., 2014)	0.022	0.16	0.014	1.6	11.4
[DMEAH][For] (Huang et al., 2014)	0.013	0.099	0.007	1.9	14.1
[emim][Tf_2N] (Sakhaeinia et al., 2010a; Hong et al., 2007)	0.006	0.060	0.047	0.13	1.3
pure MDEA[i] (Koech et al., 2011)	–	0.51	–	–	–
50 wt% MDEA Jou et al., 1982	0.30	0.85	0.72	0.42	1.2

[a] Solubility data were reported at 313.2 K unless otherwise noted.
[b] Solubility of H_2S at 0.1 bar.
[c] Solubility of H_2S at 1 bar.
[d] Solubility of CO_2 at 1 bar.
[e] Selectivity of H_2S/CO_2 defined as $R_{H2S,0.1}/R_{CO2,1}$.
[f] Selectivity of H_2S/CO_2 defined as $R_{H2S,1}/R_{CO2,1}$.
[g] Solubility data were reported at 323.2 K.
[h] Solubility data were reported at 333.2 K.
[i] Solubility data were reported at 298.2 K.

high in relative to those in carboxylate-based ILs, amino acid ILs, protic ILs, normal ILs and industrially used MDEA (0.13–1.9 for $S_{0.1/1}$ and 1.1–14.1 for $S_{1/1}$), although they are comparable as or slightly inferior to those in DLB-ILs and TA-PILs (3.9–10.4 for $S_{0.1/1}$ and 16.5–33.8 for $S_{1/1}$).

Therefore, [TMGH][PhO] is believed to be a promising candidate for the selective sweetening of natural gas because it exhibits both high solubilities of H_2S and high selectivities of H_2S/CO_2. The high solubilities of H_2S in [TMGH][PhO] origin from the strong basicity of [PhO], while the high selectivities of H_2S/CO_2 in [TMGH][PhO] origin from the strong hydrogen-bond donation of [TMGH]. Actually, another advantage of [TMGH][PhO] is its cost-effectiveness, as it can be facilely synthesized from the one-step neutralization of readily available TMG and phenol. However, many other absorbents (e.g., carboxylate-based ILs, amino acid ILs, DLB-ILs, TA-PILs and normal ILs) suffer from complex synthesis and/or expensive reactants, which could limit their applications in the industry.

3.6. Absolute solubilities of H_2S in phenolic ILs and other absorbents

The solubilities of H_2S discussed above (in terms of mol gas/mol IL) are relative solubilities. For industrial applications, the absolute solubilities of H_2S (in terms of mol gas/kg IL) are more concerned. Therefore, the absolute solubilities of H_2S in phenolic ILs are calculated in this section and summarized in Table 3. Although the relative solubilities of H_2S in the four phenolic ILs are comparable, their absolute solubilities of H_2S are different and follow the sequence of $[P_{4444}][PhO] < [hmim][PhO] < [DBUH][PhO] < [TMGH][PhO]$. For example, the absolute solubilities of H_2S in $[P_{4444}][PhO]$ are 1.76 mol/kg at 0.1 bar and 2.50 mol/kg at 1 bar, while those in [TMGH][PhO] reach 2.68 mol/kg at 0.1 bar and 4.06 mol/kg at 1 bar. Obviously, the sequence of absolute H_2S solubilities is in contrast to the sequence of molecular weight. Therefore, in addition to strong interaction with H_2S, small molecular size is also very important for functionalized ILs specifically designed for H_2S absorption.

The absolute solubilities of H_2S in other absorbents reported in the literature (Sakhaeinia et al., 2010a; Huang et al., 2013; Huang et al., 2014; Huang et al., 2014; Huang et al., 2016; Shiflett and Yokozeki, 2009; Hong et al., 2007; Koech et al., 2011; Jou et al., 1982) are also calculated and summarized in Table 3. As can be seen, other ILs can absorb only 0.015–2.54 mol/kg of H_2S at 0.1 bar and 0.15–2.84 mol/kg of H_2S at 1 bar, being much lower than the absolute solubilities of H_2S in [TMGH][PhO]. Especially for DLB-ILs and TA-PILs, which have been determined to exhibit high selectivity of H_2S/CO_2, the absolute solubilities of H_2S in them (0.25–0.56 mol/kg at 0.1 bar and 1.00–2.00 mol/kg at 1 bar) are less than half of those in [TMGH][PhO]. The absolute solubilities of H_2S in [TMGH][PhO] are even comparable to those in pure MDEA (4.32 mol/kg at 1 bar), and surpass those in 50 wt% aqueous solution of MDEA (1.26 mol/kg at 0.1 bar and 3.56 mol/kg at 1 bar). Therefore, the superiority of [TMGH][PhO] to other absorbents for H_2S absorption is more significant if the solubilities of H_2S are compared in the scale of molality, mainly as a combined result of the strong interaction of [PhO] with H_2S and the small molecular size of [TMGH][PhO]. However, other absorbents reported in the literature are either with weak interaction with H_2S or of large molecular size. Table S3 summarizes the capacities of H_2S on some bench-mark solid adsorbents reported in the literature. It can be seen that even compared with those solid adsorbents, [TMGH][PhO] is also very competitive.

Table 3
Absolute solubilities of H_2S in phenolic ILs and other absorbents[a].

Absorbents	M_w[b] (g/mol)	$M_{H2S,0.1}$[c] (mol/kg)	$M_{H2S,1}$[d] (mol/kg)
$[P_{4444}][PhO]$	352.54	1.76	2.50
[hmim][PhO]	260.38	2.27	3.23
[DBUH][PhO]	246.35	2.44	3.25
[TMGH][PhO]	209.29	2.68	4.06
[emim][Ac][e] (Huang et al., 2013; Shiflett and Yokozeki, 2009)	170.21	1.15	2.42
$[N_{2224}][Gly]$[f] (Huang et al., 2014)	232.37	2.54	2.84
$[N_{2224}][IMA]$ (Huang et al., 2014)	283.42	0.56	1.80
$[N_{2224}][NIA]$ (Huang et al., 2014)	280.41	0.43	2.00
$[BDMAEE][Tf_2N]$ (Huang et al., 2016)	441.40	0.25	1.00
$[TMHDA][Tf_2N]$ (Huang et al., 2016)	453.46	0.52	1.48
[DMEAH][Ac] (Huang et al., 2014)	135.16	0.16	1.18
[DMEAH][For] Huang et al., 2014	121.14	0.11	0.82
$[emim][Tf_2N]$ (Sakhaeinia et al., 2010a; Hong et al., 2007)	391.30	0.015	0.15
pure MDEA[g] Koech et al., 2011	119.16	–	4.32
50 wt% MDEA (Jou et al., 1982)	119.16	1.26	3.56

[a] Solubility data were determined or reported at 313.2 K unless otherwise noted.
[b] Molecular weight.
[c] Solubility of H_2S at 0.1 bar.
[d] Solubility of H_2S at 1 bar.
[e] Solubility data were reported at 323.2 K.
[f] Solubility data were reported at 333.2 K.
[g] Solubility data were reported at 298.2 K.

3.7. Solubilities of H_2S and CO_2 and selectivities of H_2S/CO_2 in [TMGH][PhO]

[TMGH][PhO] is demonstrated to have great potential in the selective sweetening of natural gas because of its high solubilities of H_2S (both high relative solubilities and high absolute solubilities), high selectivities of H_2S/CO_2 and cost-effectiveness. Therefore, the solubilities of H_2S and CO_2 in [TMGH][PhO] at different temperatures were systematically determined, as shown in Fig. 6. The measured solubilities of H_2S and calculated selectivities of H_2S/CO_2 in [TMGH][PhO] are summarized in Table 4. As can be seen, both the solubilities of H_2S and CO_2 in [TMGH][PhO] decrease with the increase of temperature. However, the variation of H_2S solubilities in [TMGH][PhO] is less sensitive to temperature than that of CO_2 solubilities in [TMGH][PhO], because the interaction of [TMGH][PhO] with H_2S (−31.9 kJ/mol) is much stronger than that with CO_2 (−11.4 kJ/mol). For example, the solubilities of H_2S in [TMGH][PhO] at 0.1 bar decrease by 32% (from 0.69 to 0.47 mol/mol or from 3.30 to 2.25 mol/kg), and the solubilities of H_2S in [TMGH][PhO] at 1 bar decrease by 20% (from 0.97 to 0.78 mol/mol or from 4.63 to 3.73 mol/kg), as the temperatures increase from 298.2 to 333.2 K. However, the solubilities of CO_2 in [TMGH][PhO] at 1 bar decrease by 53% (from 0.13 to 0.061 mol/mol), as the temperatures increase from 298.2 to 333.2 K. As a result, the selectivities of H_2S/CO_2 in [TMGH][PhO] increase with the increase of temperature. For example, the values of $S_{0.1/1}$ and $S_{1/1}$ in [TMGH][PhO] increase from 5.3 to 7.7 and from 7.5 to 12.8 respectively, as the temperatures increase from 298.2 to 333.2 K.

3.8. Recycle of [TMGH][PhO] for H_2S absorption

To evaluate the recyclability of [TMGH][PhO] for H_2S absorption, the absorption isotherm of H_2S in [TMGH][PhO] at 298.2 K was measured first. The H_2S-saturated [TMGH][PhO] was then heated to 353.2 K under a vacuum of 0.001 bar for 2 h, and reused for the measurement of H_2S absorption isotherm. The absorption-desorption cycles were performed for five times. Fig. 7 shows the solubilities of H_2S at 298.2 K and 1 bar during the five cycles. It can be seen that the absorption of H_2S in $[BDMAEE][Tf_2N]$ is totally reversible, and the solubility of H_2S remains almost unchanged after five cycles.

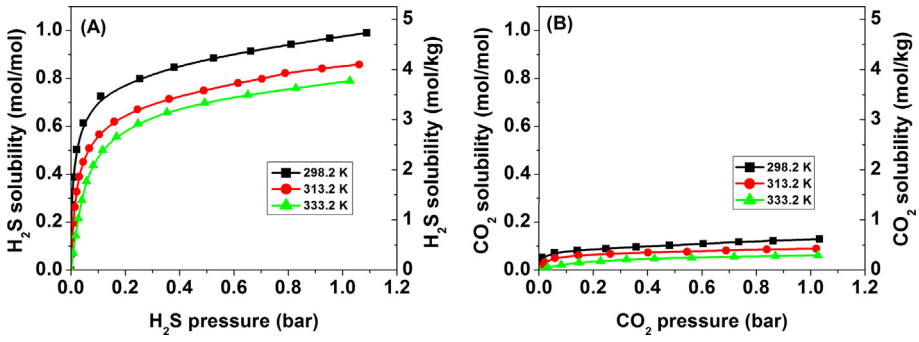

Fig. 6. Absorption isotherms of H_2S (A) and CO_2 (B) in [TMGH][PhO] at different temperatures.

Table 4
Solubilities of H_2S and selectivities of H_2S/CO_2 in [TMGH][PhO] at different temperatures.

Temperature (K)	$R_{H2S,0.1}/M_{H2S,0.1}$ [a] (mol/mol)/(mol/kg)	$R_{H2S,1}/M_{H2S,1}$ [b] (mol/mol)/(mol/kg)	$S_{0.1/1}$ [c]	$S_{1/1}$ [d]
298.2	0.69/3.30	0.97/4.63	5.3	7.5
313.2	0.56/2.68	0.85/4.06	6.2	9.4
333.2	0.47/2.25	0.78/3.73	7.7	12.8

[a] Solubility of H_2S at 0.1 bar.
[b] Solubility of H_2S at 1 bar.
[c] Selectivity of H_2S/CO_2 defined as $R_{H2S,0.1}/R_{CO2,1}$.
[d] Selectivity of H_2S/CO_2 defined as $R_{H2S,1}/R_{CO2,1}$.

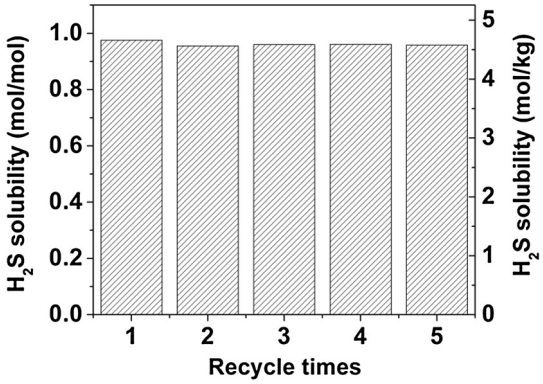

Fig. 7. Recyclability of [TMGH][PhO] for H_2S absorption.

4. Conclusions

In summary, the dependence of H_2S solubilities and CO_2 solubilities on the cationic hydrogen-bond donation of phenolic ILs were found to show different trends in this work. The solubilities of H_2S in phenolic ILs is almost independent on the cationic hydrogen-bond donation due to the ionizability of H_2S and the formation of relatively stable coplanar structures of active protons of H_2S and [PhO]. However, the solubilities of CO_2 in phenolic ILs is highly dependent on the cationic hydrogen-bond donation due to the non-ionizability of CO_2 and the formation of unstable non-coplanar structures of angular CO_2 and [PhO], and the solubilities of CO_2 in phenolic ILs decrease significantly with the increase of cationic hydrogen-bond donation. Based on this finding, highly efficient and selective absorption of H_2S from CO_2 is realized in phenolic ILs by cooperatively making use of the anionic strong basicity and cationic hydrogen-bond donation. Furthermore, cost-effectiveness and small molecular size are also proposed to be key features for functionalized ILs specifically designed for the selective sweetening of natural gas.

Acknowledgement

This work was supported by the Natural Science Foundation of Jiangxi Province (grant number: 20171BAB203019), and the Natural Science Foundation of China (grant numbers: 20806037 and 21366019). The authors also appreciate the sponsorship from Nanchang University.

Appendix A. Supplementary material

Supplementary data associated with this article can be found, in the online version, at http://dx.doi.org/10.1016/j.ces.2017.07.048.

References

Bara, J.E., 2012. Potential for hydrogen sulfide removal using ionic liquid solvents. In: Mohammad, A., Inamuddin, D. (Eds.), Green Solvents II. Springer, Netherlands, pp. 155–167.
Lawson, J.D., Garst, A.W., 1976. Gas sweetening data: equilibrium solubility of hydrogen sulfide and carbon dioxide in aqueous monoethanolamine and aqueous diethanolamine solutions. J. Chem. Eng. Data 21 (1), 20–30.
Lee, J.I., Otto, F.D., Mather, A.E., 1976. Measurement and prediction of solubility of mixtures of carbon dioxide and hydrogen sulfide in a 2.5 N monoethanolamine solution. Can. J. Chem. Eng. 54 (3), 214–219.
Sada, E., Kumazawa, H., Butt, M.A., Hayashi, D., 1976. Simultaneous absorption of carbon dioxide and hydrogen sulfide into aqueous monoethanolamine solutions. Chem. Eng. Sci. 31 (9), 839–841.
Pieplu, A., Saur, O., Lavalley, J.C., Legendre, O., Nedez, C., 1998. Claus catalysis and H_2S selective oxidation. Catal. Rev. Sci. Eng. 40 (4), 409–450.
Mandal, B.P., Biswas, A.K., Bandyopadhyay, S.S., 2004. Selective absorption of H_2S from gas streams containing H_2S and CO_2 into aqueous solutions of N-methyldiethanolamine and 2-amino-2-methyl-1-propanol. Sep. Purif. Technol. 35 (3), 191–202.
Lu, J.G., Zheng, Y.F., He, D.L., 2006. Selective absorption of H_2S from gas mixtures into aqueous solutions of blended amines of methyldiethanolamine and 2-tertiarybutylamino-2-ethoxyethanol in a packed column. Sep. Purif. Technol. 52 (2), 209–217.
Brennecke, J.F., Maginn, E.J., 2001. Ionic liquids: innovative fluids for chemical processing. AIChE J. 47 (11), 2384–2389.
Lei, Z., Dai, C., Chen, B., 2014. Gas solubility in ionic liquids. Chem. Rev. 114 (2), 1289–1326.
Fredlake, C.P., Crosthwaite, J.M., Hert, D.G., Aki, S., Brennecke, J.F., 2004. Thermophysical properties of imidazolium-based ionic liquids. J. Chem. Eng. Data 49 (4), 954–964.
Jou, F.Y., Mather, A.E., 2007. Solubility of hydrogen sulfide in [bmim][PF_6]. Int. J. Thermophys. 28 (2), 490–495.
Pomelli, C.S., Chiappe, C., Vidis, A., Laurenczy, G., Dyson, P.J., 2007. Influence of the interaction between hydrogen sulfide and ionic liquids on solubility: experimental and theoretical investigation. J. Phys. Chem. B 111 (45), 13014–13019.
Jalili, A.H., Rahmati-Rostami, M., Ghotbi, C., Hosseini-Jenab, M., Ahmadi, A.N., 2009. Solubility of H_2S in Ionic Liquids [bmim][PF_6], [bmim][BF_4], and [bmim][Tf_2N]. J. Chem. Eng. Data 54 (6), 1844–1849.
Rahmati-Rostami, M., Ghotbi, C., Hosseini-Jenab, M., Ahmadi, A.N., Jalili, A.H., 2009. Solubility of H_2S in ionic liquids [hmim][PF_6], [hmim][BF_4], and [hmim][Tf_2 N]. J. Chem. Thermodyn. 41 (9), 1052–1055.
Jalili, A.H., Mehdizadeh, A., Shokouhi, M., Ahmadi, A.N., Hosseini-Jenab, M., Fateminassab, F., 2010. Solubility and diffusion of CO_2 and H_2S in the ionic liquid 1-ethyl-3-methylimidazolium ethylsulfate. J. Chem. Thermodyn. 42 (10), 1298–1303.

Sakhaeinia, H., Jalili, A.H., Taghikhani, V., Safekordi, A.A., 2010a. Solubility of H_2S in ionic liquids 1-ethyl-3-methylimidazolium hexafluorophosphate ([emim][PF_6]) and 1-ethyl-3-methylimidazolium bis(trifluoromethyl)sulfonylimide ([emim][Tf_2 N]). J. Chem. Eng. Data 55 (12), 5839–5845.

Sakhaeinia, H., Taghikhani, V., Jalili, A.H., Mehdizadeh, A., Safekordi, A.A., khaeinia et al., 2010 b. Solubility of H_2S in 1-(2-hydroxyethyl)-3-methylimidazolium ionic liquids with different anions. Fluid Phase Equilibr. 298 (2), 303–309.

Shiflett, M.B., Niehaus, A.M.S., Yokozeki, A., 2010. Separation of CO_2 and H_2S using room-temperature ionic liquid [bmim][$MeSO_4$]. J. Chem. Eng. Data 55 (11), 4785–4793.

Shiflett, M.B., Yokozeki, A., 2010. Separation of CO_2 and H_2S using room-temperature ionic liquid [bmim][PF_6]. Fluid Phase Equilibr. 294 (1–2), 105–113.

Shokouhi, M., Adibi, M., Jalili, A.H., Hosseini-Jenab, M., Mehdizadeh, A., 2010. Solubility and diffusion of H_2S and CO_2 in the ionic liquid 1-(2-hydroxyethyl)-3-methylimidazolium tetrafluoroborate. J. Chem. Eng. Data 55 (4), 1663–1668.

Rahmati-Rostami, M., Behzadi, B., Ghotbi, C., 2011. Thermodynamic modeling of hydrogen sulfide solubility in ionic liquids using modified SAFT-VR and PC-SAFT equations of state. Fluid Phase Equilibr. 309 (2), 179–189.

Jalili, A.H., Safavi, M., Ghotbi, C., Mehdizadeh, A., Hosseini-Jenab, M., Taghikhani, V., 2012. Solubility of CO_2, H_2S, and their mixture in the ionic liquid 1-octyl-3-methylimidazolium bis(trifluoromethyl)sulfonylimide. J. Phys. Chem. B 116 (9), 2758–2774.

Chen, J.J., Li, W.W., Yu, H.Q., Li, X.L., 2013. Capture of H_2S from binary gas mixture by imidazolium-based ionic liquids with nonfluorous anions: a theoretical study. AIChE J. 59 (10), 3824–3833.

Huang, K., Cai, D.N., Chen, Y.L., Wu, Y.T., Hu, X.B., Zhang, Z.B., 2013. Thermodynamic validation of 1-alkyl-3-methylimidazolium carboxylates as task-specific ionic liquids for H_2S absorption. AIChE J. 59 (6), 2227–2235.

Jalili, A.H., Shokouhi, M., Maurer, G., Hosseini-Jenab, M., 2013. Solubility of CO_2 and H_2S in the ionic liquid 1-ethyl-3-methylimidazolium tris(pentafluoroethyl) trifluorophosphate. J. Chem. Thermodyn. 67, 55–62.

Mortazavi-Manesh, S., Satyro, M.A., Marriott, R.A., 2013. Screening ionic liquids as candidates for separation of acid gases: solubility of hydrogen sulfide, methane, and ethane. AIChE J. 59 (8), 2993–3005.

Safavi, M., Ghotbi, C., Taghikhani, V., Jalili, A.H., Mehdizadeh, A., 2013. Study of the solubility of CO_2, H_2S and their mixture in the ionic liquid 1-octyl-3-methylimidazolium hexafluorophosphate: experimental and modelling. J. Chem. Thermodyn. 65, 220–232.

Ahmadi, M.A., Haghbakhsh, R., Soleimani, R., Bajestani, M.B., 2014. Estimation of H_2S solubility in ionic liquids using a rigorous method. J. Supercrit. Fluids 92, 60–69.

Faundez, C.A., Diaz-Valdes, J.F., Valderrama, O.J., 2014. Testing solubility data of H_2S and SO_2 in ionic liquids for sulfur-removal processes. Fluid Phase Equilibr. 375, 152–160.

Huang, K., Zhang, X.M., Xu, Y., Wu, Y.T., Hu, X.B., Xu, Y., 2014. Protic ionic liquids for the selective absorption of H_2S from CO_2: thermodynamic Analysis. AIChE J. 60 (12), 4232–4240.

Ji, X.Y., Held, C., Sadowski, G., 2014. Modeling imidazolium-based ionic liquids with ePC-SAFT: part II. application to H2S and synthesis-gas components. Fluid Phase Equilibr. 363, 59–65.

Ahmadi, M.A., Pouladi, B., Javvi, Y., Alfkhani, S., Soleimani, R., 2015. Connectionist technique estimates H_2S solubility in ionic liquids through a low parameter approach. J. Supercrit. Fluids. 97, 81–87.

Haghtalab, A., Afsharpour, A., 2015. Solubility of CO_2+H_2S gas mixture into different aqueous N-methyldiethanolamine solutions blended with 1-butyl-3-methylimidazolium acetate ionic liquid. Fluid Phase Equilibr. 406, 10–20.

Haghtalab, A., Kheiri, A., 2015. High pressure measurement and CPA equation of state for solubility of carbon dioxide and hydrogen sulfide in 1-butyl-3-methylimidazolium acetate. J. Chem. Thermodyn. 89, 41–50.

Hamzehie, M.E., Fattahi, M., Najibi, H., Van der Bruggen, B., Mazinani, S., 2015. Application of artificial neural networks for estimation of solubility of acid gases (H_2S and CO_2) in 32 commonly ionic liquid and amine solutions. J. Nat. Gas Sci. Eng. 24, 106–114.

Sanchez-Badillo, J., Gallo, M., Alvarado, S., Glossman-Mitnik, D., 2015. Solvation Thermodynamic properties of hydrogen sulfide in [C_4mim][PF_6], [C_4mim][BF_4], and [C_4mim][Cl] ionic liquids, determined by molecular simulations. J. Phys. Chem. B 119 (33), 10727–10737.

Wang, B., Zhang, K., Ren, S., Hou, Y., Wu, W., 2016. Efficient capture of low partial pressure H_2S by tetraethyl ammonium amino acid ionic liquids with absorption-promoted solvents. RSC Adv. 6 (103), 101462–101469.

Zhao, Y., Gao, H., Zhang, X., Huang, Y., Bao, D., Zhang, S., 2016. Hydrogen sulfide solubility in ionic liquids (ILs): an extensive database and a new ELM model mainly established by imidazolium-based ILs. J. Chem. Eng. Data 61 (12), 3970–3978.

Afsharpour, A., Haghtalab, A., 2017. Simultaneous measurement absorption of CO_2 and H_2S mixture into aqueous solutions containing diisopropanolamine blended with 1-butyl-3-methylimidazolium acetate ionic liquid. Int. J. Greenh. Gas Con. 58, 71–80.

Soltani Panah, H., 2017. Modeling H_2S and CO_2 solubility in ionic liquids using the CPA equation of state through a new approach. Fluid Phase Equilibr. http://dx.doi.org/10.1016/j.fluid.2017.01.023. in press.

Huang, K., Wu, Y.T., Hu, X.B., 2016. Effect of alkalinity on absorption capacity and selectivity of SO_2 and H_2S over CO_2: substituted benzoate-based ionic liquids as the study platform. Chem. Eng. J. 297, 265–276.

Huang, K., Cai, D.N., Chen, Y.L., Wu, Y.T., Hu, X.B., Zhang, Z.B., 2014. Dual lewis-base functionalization of ionic liquids for highly efficient and selective capture of H_2S. ChemPlusChem 79 (2), 241–249.

Huang, K., Zhang, X.M., Hu, X.B., Wu, Y.T., 2016. Hydrophobic protic ionic liquids tethered with tertiary amine group for highly efficient and selective absorption of H_2S from CO_2. AIChE J. 62, 4480–4490.

Wang, C., Luo, H., Li, H., Zhu, X., Yu, B., Dai, S., 2012. Tuning the physicochemical properties of diverse phenolic ionic liquids for equimolar CO_2 capture by the substituent on the anion. Chem. Eur. J. 18 (7), 2153–2160.

Frisch MJ, Trucks GW, Schlegel HB, Scuseria GE, Robb MA, Cheeseman JR, Montgomery JA, Vreven T, Kudin KN, Burant JC, Millam JM, Iyengar SS, Tomasi J, Barone V, Mennucci B, Cossi M, Scalmani G, Rega N, Petersson GA, Nakatsuji H, Hada M, Ehara M, Toyota K, Fukuda R, Hasegawa J, Ishida M, Nakajima T, Honda Y, Kitao O, Nakai H, Klene M, Li X, Knox JE, Hratchian HP, Cross JB, Adamo C, Jaramillo J, Gomperts R, Stratmann RE, Yazyev O, Austin AJ, Cammi R, Pomelli C, Ochterski JW, Ayala PY, Morokuma K, Voth GA, Salvador P, Dannenberg JJ, Zakrzewski VG, Dapprich S, Daniels AD, Strain MC, Farkas O, Malick DK, Rabuck AD, Raghavachari K, Foresman JB, Ortiz JV, Cui Q, Baboul AG, Clifford S, Cioslowski J, Stefanov BB, Liu G, Liashenko A, Piskorz P, Komaromi I, Martin RL, Fox DJ, Keith T, Al-Laham MA, Peng CY, Nanayakkara A, Challacombe M, Gill PMW, Johnson B, Chen W, Wong MW, Gonzalez C, Pople JA. Gaussian 09. Pittsburgh, PA, Gaussian, Inc., 2009.

Greaves, T.L., Drummond, C.J., 2008. Protic ionic liquids: properties and applications. Chem. Rev. 108 (1), 206–237.

Zhang, X.M., Huang, K., Xia, S., Chen, Y.L., Wu, Y.T., Hu, X.B., 2015. Low-viscous fluorine-substituted phenolic ionic liquids with high performance for capture of CO_2. Chem. Eng. J. 274, 30–38.

Shang, D., Zhang, X., Zeng, S., et al., 2017. Protic ionic liquid [Bim][NTf_2] with strong hydrogen bond donating ability for highly efficient ammonia absorption. Green Chem. http://dx.doi.org/10.1039/C6GC03026B. in press.

Kaljurand, I., Rodima, T., Leito, I., Koppel, I.A., Schwesinger, R., 2000. Self-consistent spectrophotometric basicity scale in acetonitrile covering the range between pyridine and DBU. J. Org. Chem. 65 (19), 6202–6208.

Lide, D.R., 2003. CRC Handbook of Chemistry and Physics. CRC Press, Boca Raton, Florida.

Zhang, X.M., Bordwell, F.G., Vanderpuy, M., Fried, H.E., 1993. Equilibrium acidities and homolytic bond-dissociation energies of the acidic C—H bonds in N-substituted trimethylammonium and pyridinium cations. J. Org. Chem. 58 (11), 3060–3066.

Magill, A.M., Cavell, K.J., Yates, B.F., 2004. Basicity of nucleophilic carbenes in aqueous and nonaqueous solvents-theoretical predictions. J. Am. Chem. Soc. 126 (28), 8717–8724.

Shiflett, M.B., Yokozeki, A., 2009. Phase behavior of carbon dioxide in ionic liquids: [emim][acetate], [emim][trifluoroacetate], and [emim][acetate] plus [emim][trifluoroacetate] mixtures. J. Chem. Eng. Data 54 (1), 108–114.

Hong, G., Jacquemin, J., Deetlefs, M., Hardacre, C., Husson, P., Gomes, M.F.C., 2007. Solubility of carbon dioxide and ethane in three ionic liquids based on the bis{(trifluoromethyl)sulfonyl}imide anion. Fluid Phase Equilibr. 257 (1), 27–34.

Koech, P.K., Rainbolt, J.E., Bearden, M.D., Zheng, F., Heldebrant, D.J., 2011. Chemically selective gas sweetening without thermal-swing regeneration. Energy Environ. Sci. 4 (4), 1385–1390.

Jou, F.Y., Mather, A.E., Otto, F.D., 1982. Solubility of H_2S and CO_2 in aqueous methyldiethanolamine solutions. Ind. Eng. Chem. Process Des. Dev. 21 (4), 539–544.